Macromolecules

ARTICLE

pubs.acs.org/Macromolecules

Sorbitol−POSS Interactions on Development of Isotactic Polypropylene Composites

Sayantan Roy,[†] Vincenzo Scionti,[‡] Sadhan C. Jana,*[,†] Chrys Wesdemiotis,[‡] Anna M. Pischera,[‡] and Mathew P. Espe[‡]

[†]Department of Polymer Engineering, The University of Akron, Akron, Ohio 44325-0301, United States

[‡]Department of Chemistry, The University of Akron, Akron, Ohio 44325-3601, United States

Supporting Information

ABSTRACT: This study investigates the nature of interactions between the molecules of polyhedral oligomeric silsesquioxane (POSS) containing silanol functionalities (silanol−POSS) and di(benzylidene)sorbitol (DBS) encountered in the development of nanocomposite fibers from the compounds of POSS, DBS, and isotactic polypropylene (iPP). The interactions were investigated using Fourier transform infrared (FTIR) spectroscopy, differential scanning calorimetry (DSC), wide-angle X-ray diffraction (WAXD), nuclear magnetic resonance (NMR) spectroscopy, mass spectrometry, and oscillatory shear rheology. Mass and NMR spectrometry revealed that the molecules of silanol−POSS and DBS formed several amorphous noncovalent molecular complexes promoted by hydrogen bonding. More abundant complex formation was observed with silanol−POSS molecules carrying four silanol groups and phenyl substitutions. Such complex formation deterred fibrillation of DBS when the compounds of iPP, DBS, and silanol−POSS were cooled from homogeneous melt states. It was also revealed that POSS−DBS complexes were of much lower viscosity than iPP.

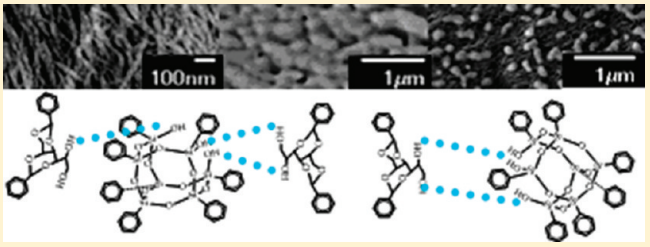

INTRODUCTION

In recent years polyhedral oligomeric silsesquioxanes (POSS) have received considerable attention as hybrid organic−inorganic filler materials for development of polymer nanocomposites.[1−18] In comparison with more conventional inorganic fillers, such as talc, layered silicate clay, and silica, POSS molecules are more promising due to the advantage of monodispersed size ranging between 1 and 3 nm, isotropic molecular shape, low density, high thermal stability, and an array of functionalities.[19−21] POSS molecules can be functionalized to aid incorporation in several polymer systems via copolymerization and grafting reactions and to render them as integral parts of polymer chains.[7,19,20] While such reactions are beneficial in designing specific molecular structures, their usage in development of POSS−polymer composites suffers from several inherent limitations, such as deterioration of mechanical properties.[7]

Melt blending of nonreactive POSS molecules with the host polymers presents a much simpler alternative to grafting and copolymerization reactions for preparation of POSS−polymer nanocomposites.[1,2,6,9,11,13−17] Nonreactive POSS molecules are easier to synthesize and can be mixed with the polymer using an array of extruders and internal mixers. However, good dispersion and desired improvements in mechanical properties strongly depend on POSS−polymer compatibility.[6,22] In this study, a set of incompletely condensed[23−30] POSS molecules bearing multiple polar silanol groups (Si−OH), henceforth silanol−POSS, were compounded with isotactic polypropylene (iPP) for development of nanocomposite fibers with substantial reduction in fiber diameter and large enhancement in tensile properties.

It was recognized at the outset that the polar nature of silanol−POSS would deter its dispersion in iPP melt. To circumvent this, up to 1 wt % of a sorbitol-type nucleating agent was added in the compounds. It was hypothesized that stronger sorbitol−POSS hydrogen-bonding interactions would promote dispersion of silanol−POSS in iPP melt and that the fibrillar networks of sorbitol formed upon cooling would serve as templates for assembly of silanol−POSS molecules into nanoparticles. This paper investigated the nature of sorbitol−POSS interactions using several analytical tools.

The free −OH groups in sorbitol can form both intramolecular and intermolecular self-assembled superstructures via hydrogen bonding. The hydrophobic aromatic rings in sorbitol are known to promote compatibility with polyolefins.[31,32] Sorbitol molecules get completely dissolved and homogeneously dispersed in molten iPP. Upon cooling, a transient gel is formed with endless, thin, twisted fibrils of sorbitol which nucleate crystallization of iPP chains. It was reported that homogeneous melt mixtures of di(benzylidene)sorbitol (DBS) and iPP upon cooling result in elementary DBS fibers of typical diameter ∼10 nm.[33,34] A similar phenomenon was identified for di(dimethylbenzylidene)sorbitol (DMDBS).[35] The self-aggregation

Received: July 12, 2011
Revised: September 9, 2011
Published: September 22, 2011

ACS Publications © 2011 American Chemical Society

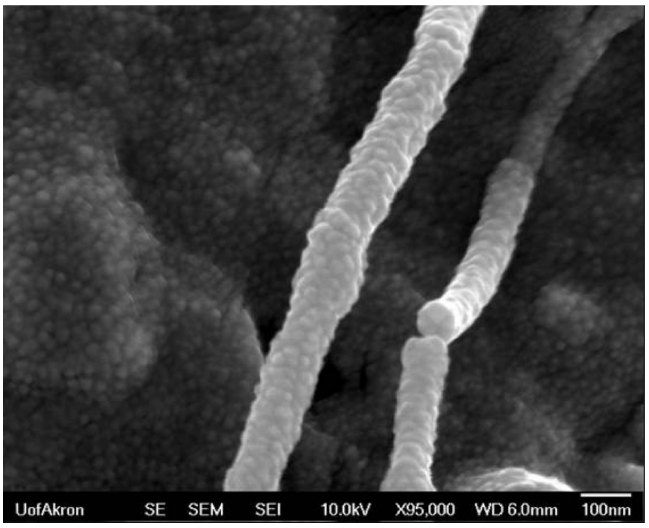

Figure 1. Scanning electron microscope image of fractured surface of melt-spun fiber (draw ratio 380) of iPP compound containing DBS/trisilanol phenyl-POSS 1/5 wt/wt processed at 200 °C.

of sorbitol molecules such as DBS is believed to be the result of intermolecular hydrogen bonding[34] and $\pi-\pi$ interactions between the adjacent phenyl rings.[36,37] Highly organized fibrillar bundles of DBS are formed up to a concentration of 1−2 wt %, beyond which DBS remains insoluble in molten iPP.[35,38,39]

POSS-type organosilanols have been known to form useful building blocks for supramolecular chemistry; complexes based on silanols have been reported in the literature.[23,40,41] Our previous work[42−45] reported that dispersion of nonreactive trisilanol phenyl-POSS (tri-POSS) in iPP can be improved in the presence of DBS. These studies also reported that in the presence of tri-POSS the fibrillar networks of DBS did not form easily when compounds were cooled from a homogeneous melt state. This was attributed to stronger interactions between silanol−POSS and DBS than DBS−DBS interactions. This paper expanded the scope to other silanol−POSS molecules, e.g., with four silanol groups per molecule or cyclopentyl substitution instead of phenyl. The study investigated POSS−sorbitol interactions as a function of the mass ratio of sorbitol derivatives and silanol−POSS. Both DBS and DMDBS systems were investigated, but the results of tests involving DBS formed the major part of this paper. Only selected sets of data with DMDBS are presented as trends were similar to DBS. Some additional data on DMDBS are provided as Supporting Information. Our preference for DBS stemmed from its simpler molecular structure, convenient solution preparation, and lower melting temperature.

We present below a rationale for devoting this paper to the study of POSS−DBS interactions. Some reasons for not presenting the details of how such interactions impacted the properties of iPP compounds are also given. Figure 1 presents scanning electron microscope image of fractured surface of a fiber of iPP compound containing 5 wt % trisilanol phenyl-POSS and 1 wt % DBS, melt-spun at 200 °C to a draw ratio of 380. The compound was prepared by mixing the ingredients in a batch mixer at 190 °C for 5 min. These fibers with 93 μm mean diameter offered ∼2 GPa tensile modulus and 100 MPa tensile strength. The same compound, spun to a minimum mean diameter of 40 μm, offered tensile modulus of 4 GPa and tensile strength of 190 MPa. It was found that the presence of DBS and trisilanol phenyl-POSS in the compound allowed melt spinning to a maximum draw ratio of about 2000 compared to a maximum draw ratio of about 800 for iPP alone. The cylindrical particles of ∼100 nm in diameter seen at the center of the image in Figure 1 were formed from an amorphous, liquid molecular complex of trisilanol phenyl-POSS and DBS after it underwent substantial stretching during fiber spinning. As will be described in the Experimental Section, both trisilanol phenyl-POSS and DBS are crystalline solids at 200 °C and should not have formed a deformable liquid on their own. A detailed treatment of the effects of the POSS−DBS molecular complexes on fiber draw ratio during melt spinning and fiber mechanical properties warrants a separate publication which will be communicated elsewhere. Instead, the present paper focuses on the nature of these molecular complexes.

The following specific issues were investigated in this paper. In our previous work,[42−45] an indirect evidence of interactions between tri-POSS and DBS molecules was gleaned from the rheological data, and such interactions were attributed to hydrogen bonding. However, it was not studied if the number of Si−OH groups or the nature of organic substitutions in silanol−POSS molecules would have any impact on such interactions. It was also not investigated if POSS−sorbitol interactions would lead to molecular complex formation or if such complexes were indeed chemical compounds. The study also determined various POSS−DBS molecular adducts in the complex and reported minimum quantities of POSS required to form complex with DBS. The issue of molecular complex formation was found to be very relevant in making nanocomposite fibers from the compounds of iPP, DBS, and silanol−POSS as reflected in the preceding paragraph. The complex may not show crystalline order and instead may exhibit amorphous nature with glass transition temperature much lower than the crystalline melting temperature of iPP. This in turn may facilitate fiber spinning of the compounds. For example, a POSS−DBS complex, due to low viscosity in liquid state at or above iPP melting temperature, may deform into large surface area cylindrical domains during fiber spinning, as seen from a representative image in Figure 1.

EXPERIMENTAL SECTION

Materials. Isotactic polypropylene, P4G2Z-159, was obtained in the form of pellets from Flint Hill Resources (Wichita, KS) with MFI 1.95 g/10 min (ASTM D1238), density 0.90 g/cm^3 (ASTM D1505), and crystalline melting temperature (T_m) 165 °C. As per the information obtained from the supplier, this grade of iPP did not contain any nucleating agent. Three grades of silanol POSS were obtained from Hybrid Plastics (Hattiesburg, MS). Tetrasilanol phenyl-POSS (tetra-POSS, SO 1460) was available in the form of a white powder, with molecular weight 1069.5 g/mol and T_m of 260 °C. Trisilanol phenyl-POSS (tri-POSS, SO 1458) was a white powder with molecular weight of 930.07 g/mol and T_m of 230 °C. Trisilanol cyclopentyl-POSS (cyclo-POSS; SO 1430) was obtained as a white powder with molecular weight of 874.7 g/mol and T_m of 250 °C. Figure 2a−c presents the chemical structures of the silanol POSS molecules. Note that both tri-POSS and cyclo-POSS have three silanol groups, but they differ in the nature of side groups—phenyl in the case of tri-POSS and cyclopentyl in the case of cyclo-POSS.

The sorbitols chosen for this study were di(benzylidene)sorbitol (DBS; Millad 3905; M_w = 358.4 g/mol and T_m = 225 °C) and di(dimethylbenzylidene)sorbitol (DMDBS; Millad 3988; M_w = 414.49 g/mol and T_m = 275 °C). Both DBS and DMDBS have two free −OH

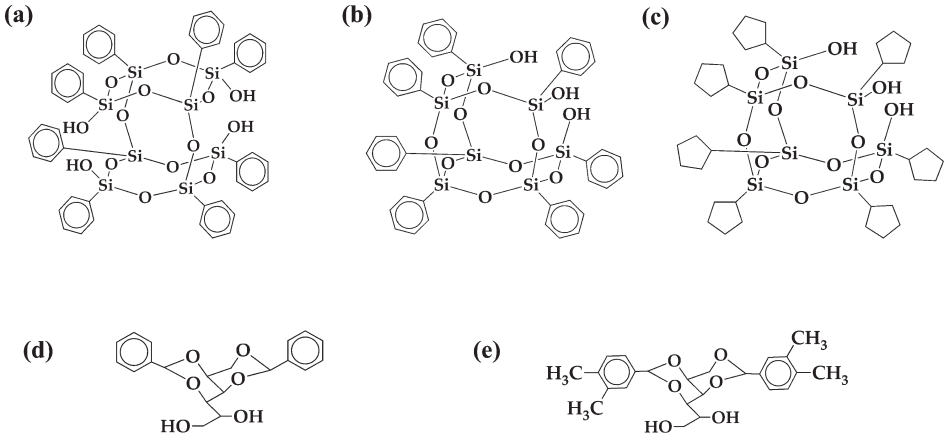

Figure 2. Chemical structures of (a) tetra-POSS, (b) tri-POSS, (c) cyclo-POSS, (d) DBS, and (e) DMDBS.

groups and phenyl side rings and have been used as clarifying agents of iPP, although DMDBS is more frequently used due to its higher melting temperature. DMDBS molecules contain two methyl substituents in each phenyl ring and melt at 50 °C higher temperature than DBS. The structures of these molecules are shown in Figure 2d,e. These materials were obtained from Milliken Chemicals (Spartanburg, SC) in the form of white powder. A majority of the data presented in this paper involve DBS as many trends with DMDBS were found to be similar to DBS.

Preparation of Sorbitol−POSS Mixtures. DBS or DMDBS and POSS were intimately mixed at different weight ratios in solution in tetrahydrofuran (THF). The solvent was evaporated, and the resultant materials were ground and vacuum-dried. One part of the mixture was kept in the oven at 200 °C for 5 min to imitate the thermal history experienced in typical polymer compound preparation and melt spinning experiments. The resultant materials were cooled to room temperature and ground into powder forms for further analysis.

Characterization. Infrared spectroscopy was used to identify POSS−POSS and POSS−sorbitol hydrogen-bonding interactions at room temperature and as a function of temperature both during heating and cooling. For this purpose, powder samples of DBS or DMDBS and POSS were compressed with potassium bromide (KBr) powder in vacuum compression mold. Fourier transform infrared (FTIR) spectra were recorded in transmission mode from 4000 to 500 cm^{-1} in a Perkin-Elmer 16 PC FTIR setup. The FTIR spectra were also recorded by placing the KBr disk inside a heating stage and changing the temperature from 45 to 200 °C at a scanning rate of 10 °C/min and also while cooling to 45 at 10 °C/min.

Thermal Analysis. The melting behavior of POSS, DBS, or DMDBS and their mixtures was investigated by differential scanning calorimetry (DSC) using DSC200 (TA Instruments) calorimeter under continuous nitrogen purge at a flow rate of 50 mL/min. The thermal properties such as T_m, glass transition temperature (T_g), and enthalpy change (ΔH_m) in melting were determined at a heating rate of 10 °C/min from 30 to 300 °C.

Wide-Angle X-ray Diffraction. Wide-angle X-ray diffraction (WAXD) of DBS or DMDBS, POSS, and their mixtures produced by mixing in solution and with heat history were investigated using Bruker wide-angle X-ray instrument with sealed tube X-ray generator and Cu Kα radiation of wavelength (λ) of 1.54 Å. The WAXD patterns were examined to determine if POSS−DBS mixtures remained crystalline or turned amorphous.

Scanning Electron Microscopy. The morphology of POSS−DBS or DMDBS mixture was observed by high-resolution scanning electron microscopy (SEM) using a JEOL JSM5310 scanning electron microscope. For this purpose, POSS, DBS (or DMDBS), and their mixtures were solution cast to reveal the self-assembled structures. The surface of the specimens was sputter-coated by a layer of silver using a sputter coater, Model ISI 5400, under argon gas atmosphere.

Mass Spectrometry. The samples designated for mass spectrometry (MS) and ion mobility mass spectrometry (IMMS) analysis were completely dissolved in THF. An aliquot of methanol (MeOH) was added to the sample solution in order to get a final concentration of 0.1 mg/mL in 1:1 (v:v) THF/MeOH.

All MS measurements were carried out using a SYNAPT HDMS hybrid quadrupole/time-of-flight (Q/oa-ToF) mass spectrometer (Waters, Beverly, MA) equipped with a Z-spray electrospray source.[46] The instrumental settings were optimized to minimize dissociation of the complexes due to the energy provided during the ionization. The instrument was operated in positive mode using the following settings: capillary voltage 3.5 kV, cone voltage 35 V, sampling cone voltage 3.2 V, source temperature 60 °C, and desolvation gas temperature 100 °C. The sample solutions were electrosprayed by direct infusion at a flow rate of 15 μL/min.

The ion mobility mass spectrometry (IMMS) experiments were performed on the same instrument by activating the traveling wave (T-Wave) separation section located between the two analyzers. This section consists of three cells in the order trap cell, ion mobility cell, and transfer cell. Once the ions generated in the source or by fragmentation in the trap cell (vide infra) enter the ion mobility cell, they move under the influence of a traveling wave electric field, in the presence of a drift gas (N_2) which flows in the opposite direction of the ions motion. Separation takes place according to the size, shape, and charge state of the ions.[47] These parameters determine the drift times of the ions through the ion mobility cell, which can be measured and converted to experimental collision cross section that reflects ion shape and size. The electric field used in the ion mobility experiments was generated by tuning the traveling wave velocity and the traveling wave height at 350 m/z and 15 V, while the nitrogen gas flow rate was set at 22.7 mL/min. For tandem mass spectrometry (MS/MS) studies, with or without TWIM separation, a specific noncovalent complex was first mass-selected by the quadrupole and then fragmented in the trap collision cell using argon as collision gas. The collision energy applied to disrupt the complexes under study was varied in the range from 6 to 20 eV, depending on the type of complex, POSS−POSS or POSS-DBS, and its stoichiometry. The fragments were mass-analyzed by the ToF analyzer either without or with prior TWIM separation.

NMR Spectroscopy. Solid-state ^{29}Si (79.4 MHz) and ^{13}C (100.5 MHz) NMR spectra were collected on a Varian INOVA 400 MHz (9.4T) spectrometer using a Varian 4 mm DR-T3 probe. Samples were packed into 4 mm ceramic rotors, and all spectra were collected with

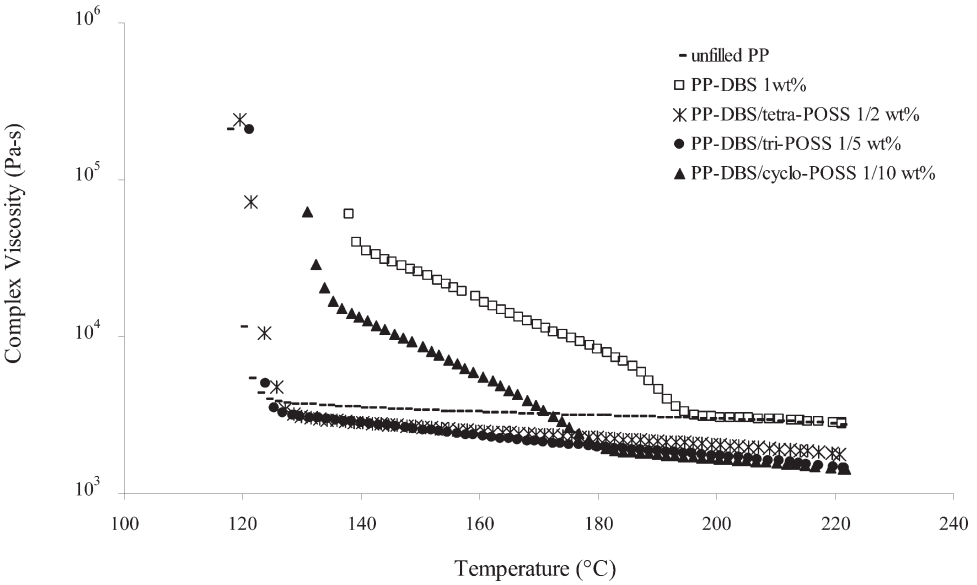

Figure 3. Temperature dependence of complex viscosity of PP compounds. The data were taken at 2% strain and frequency of 10 rad/s.

magic-angle spinning (MAS) and a spinning speed of 12 kHz. Cross-polarization (CP) $^{1}H-^{29}Si$ and $^{1}H-^{13}C$ data were acquired using ^{1}H 90° pulse widths of 5.0 and 4 μs, respectively. The B_1 fields for ^{13}C and ^{29}Si were mismatched from the Hartman−Hahn matching condition by the MAS spinning speed. Recycle delays of 2 and 5 s and CP spin-lock times of 5 and 1 ms were used for the $^{1}H-^{29}Si$ and $^{1}H-^{13}C$ experiments, respectively. ^{29}Si chemical shifts were referenced to 2,2-dimethyl-2-silapentanesulfonate (1.46 ppm), and ^{13}C chemical shifts were referenced to hexamethylbenzene (17.3 ppm, methyl).

Polymer Compound Preparation. A series of iPP/DBS or DMDBS/POSS compounds were produced in an internal mixer, Brabender Plasticorder. Before mixing, all ingredients were dried for 24 h at 80 °C in vacuum. First, PP was allowed to melt in the mixer, and then dry-blended powder mixture of DBS or DMDBS and POSS was added in the mixing chamber. The ingredients were mixed for 5 min at 200 °C at an angular speed of 80 rpm. The resultant compound was cooled down to room temperature and ground into small pellets for further analysis.

Rheological Analysis. An Advanced Rheometric Expansion System (ARES) from TA Instruments (New Castle, DE) operated with 25 mm parallel plate setup was used to measure the temperature dependence of complex viscosity of the polymer compounds in the range of 100−220 °C upon cooling from a homogeneous state at 220 °C. Disk-shaped specimens of 25 mm diameter and 2 mm thickness were molded at 200 °C in a compression mold. The specimens were subjected to 200 °C only for 5 min during molding. The polymer compound in the rheometer was first heated and kept at 220 °C for 5 min to reach equilibrium and was cooled down to 120 °C at a cooling rate of 10 °C/min. The strain was kept fixed at 2%, and the frequency of oscillatory shear flow was kept at 10 rad/s. A linear viscoelastic regime was independently confirmed under these conditions.

■ RESULTS AND DISCUSSION

Effect of POSS on DBS Fibrillation. The oscillatory shear rheological data provided the first sign of interactions between DBS and POSS as the compounds of iPP, DBS, and POSS were cooled from a homogeneous state at 220 °C. Figure 3 shows the values of complex viscosity as a function of temperature for samples containing different types and amounts of POSS. The onset of crystallization in unfilled iPP was inferred from a sudden and abrupt increase in complex viscosity at 120 °C, while DBS in iPP-DBS compound caused a distinct increase in viscosity at ∼190 °C prior to crystallization of iPP. This was due to formation of nanofibrillar networks by crystallized DBS in the polymer melt.[31,44,45]

DBS fibrillation was subdued in compounds of 5 wt % tri-POSS or 2 wt % tetra-POSS as the viscosity did not show an abrupt increase until iPP began crystallizing at 120 °C (Figure 3). This was also observed previously in compounds of iPP, DBS, and tri-POSS.[44] We then determined the minimum amount of silanol−POSS required to subdue DBS fibrillation. For this purpose, the amount of tri-POSS and tetra-POSS was varied in steps of 0.5 wt %, and the oscillatory shear viscosity data of the compounds were examined. It was found that a minimum of 2 wt % tetra-POSS or 5 wt % of tri-POSS was needed for complete suppression of fibrillation of 1 wt % DBS. The compound of 10 wt % cyclo-POSS exhibited an upturn of viscosity at ∼181 °C due to DBS fibrillation (Figure 3), indicating much less interaction with DBS.

One additional silanol group per molecule of tetra-POSS may explain why much less tetra-POSS (2 wt %) than tri-POSS (5 wt %) was needed to subdue DBS fibrillation. However, cyclo-POSS and tri-POSS have the same number of silanol groups per molecule. Nevertheless, DBS fibrillation was not completely subdued even in the presence of 10 wt % cyclo-POSS (Figure 3). This indicates that hydrogen-bonding interactions were not the only interactions possible in compounds of tri-POSS and tetra-POSS. It has been reported that DBS fibrils are composed solely of DBS molecules.[36] Thus, cessation of DBS fibrillation in the presence of tri-POSS and tetra-POSS would indicate higher affinity of DBS to these POSS molecules. It is also noted that structural flexibility of DBS molecules[37] may facilitate intermolecular hydrogen bonding with silanol POSS molecules.

Hydrogen Bonding from IR Spectra. The FTIR spectra of POSS and POSS−DBS mixtures were studied to infer POSS−POSS, POSS−DBS, and DBS−DBS hydrogen-bonding possibilities. The O−H stretching peak of Si−OH groups in tetra-POSS, tri-POSS, and cyclo-POSS are found respectively at 3288,

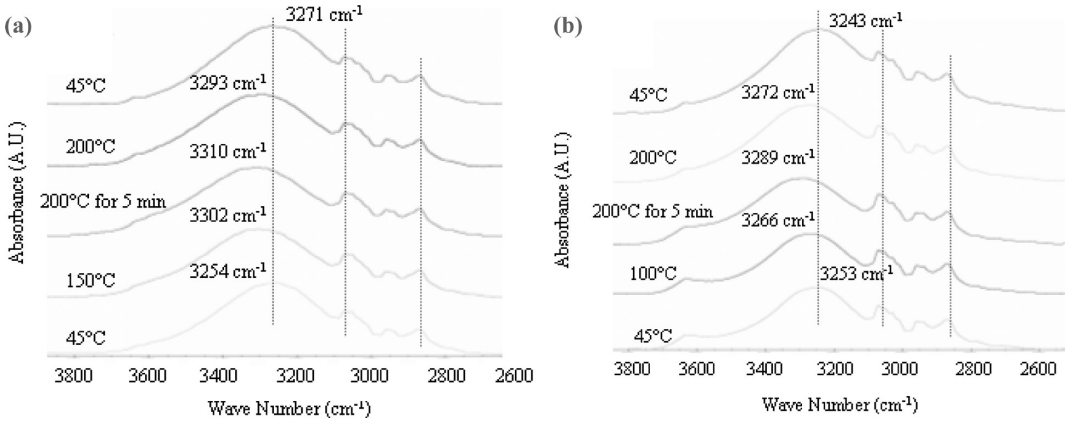

Figure 4. FTIR spectra taken during temperature sweep: (a) DBS/tetra-POSS and (b) DBS/tri-POSS (DBS/POSS 1/2 wt/wt).

3280, and 3200 cm^{-1}. It was earlier reported that tri-POSS has a strong tendency to form aggregates through hydrogen bonding in the solid state.[24,45] DBS is reported to have a C−OH stretching peak at 3220 cm^{-1}.[34]

Although the O−H stretching peak was found in POSS−DBS mixtures, the peaks originating from DBS−DBS, POSS−POSS, or POSS−DBS interactions could not be clearly distinguished (see S1 in the Supporting Information). A relatively small shift in the wavenumber of O−H stretching could be attributed to DBS−POSS interactions, but the relative strength of such interactions over POSS−POSS interactions was small. In view of this, the sample specimens were subjected to ramp heating and cooling in the IR setup to evaluate if various hydrogen bonds would show sensitivity to higher temperature and hence could be identified.

The FTIR spectra were taken as the materials were heated from room temperature to 200 °C and kept at this temperature for 5 min to imitate the typical temperature history of compound preparation and then cooled to 45 °C. The peak location and height of O−H stretching were monitored as a function of temperature. The spectra for mixtures of tetra-POSS and tri-POSS with DBS are shown in Figure 4. It is seen that hydrogen bonds weakened with heating as the O−H stretching peak location shifted to higher wavenumbers with the increase of temperature. The hydrogen bonds became stronger again upon cooling as evident from the shifting of wavenumber to lower values for all DBS/POSS combinations. A similar result was obtained for DBS−cyclo-POSS mixture. The wavenumber changed from 3218 to 3281 cm^{-1} as the material was kept at 200 °C for 5 min and then reduced to 3240 cm^{-1} as the specimen was cooled to 45 °C. These results indicate that hydrogen bonding in DBS−POSS systems weakened at the processing temperature but reappeared when the compounds were cooled down. The FT-IR data presented in Figure 4 could not answer if DBS−POSS hydrogen bonds were stronger than POSS−POSS or DBS−DBS bonds. It was then hypothesized that POSS−DBS interactions at room temperature would affect the crystalline order of both DBS and silanol−POSS molecules and that an evidence of the loss of crystalline order would indicate stronger POSS−DBS interactions. In view of this, differential scanning calorimetry and WAXD data of POSS−DBS compounds were analyzed.

Investigation of Crystallinity and Crystalline Order. POSS−DBS mixtures were prepared in solution and then dried. The data in Table 1 show that DBS, DMDBS, and POSS were crystalline. A depression in melting point of tetra-POSS and tri-POSS was observed with the addition of DBS (Table 2). Two melting transitions were also identified in mixtures at higher weight ratios of POSS, for example, broad peaks at 148 and 261 °C in the case of 1:30 wt ratio of DBS and tetra-POSS or at 142 and 210 °C in the case of 1:30 wt ratio of DBS and tri-POSS. The lower melting POSS−sorbitol mixtures possibly contained smaller crystals, which will be analyzed and verified using WAXD. Some representative DSC traces are presented in Figures 5, 6, and 7. Let us now examine the effect of heating of DBS, POSS, and DBS−POSS mixtures at 200 °C for 5 min. This would imitate the changes occurring during preparation of POSS, DBS, and iPP compounds, which in turn influenced the rheological behavior in Figure 3.

Table 1. DSC Data on Melting and Glass Transition of As-Received Specimens and after Heating at 200 °C for 5 min (Heated)

component	status	melting transition; T_m(°C)	ΔH (J/g)	T_g (°C)
DBS	as-received	sharp; 227	146	
	heated	sharp; 223	113	
DMDBS	as-received	sharp; 276	207	
	heated	sharp; 276	164	
tri-POSS	as-received	sharp; 227	71	
	heated	no melting transition		132
cyclo-POSS	as-received	sharp; 242	108	
	heated	no melting transition		211

The mixtures of tri-POSS and DBS turned into clear liquid possibly due to formation of a complex when heated at 200 °C for 5 min. The liquid was found to be Newtonian with steady shear viscosity of ∼0.5 Pa·s at 180 °C for 2:1 wt/wt tri-POSS/DBS mixture and 5 Pa·s for 5:1 wt/wt tri-POSS/DBS mixture. This is in stark contrast to viscosity of molten iPP of ∼2000 Pa·s at 180 °C. Upon cooling to room temperature, the liquid turned into transparent solid with distinct glass transition temperature, e.g., 106 and 122 °C respectively for 5:1 and 30:1 wt/wt tri-POSS/DBS mixture. A similar phenomenon was observed in the case of tetra-POSS. It formed a clear liquid upon heating at 200 °C with DBS up to tetra-POSS/DBS weight ratio of 5:1. It was revealed from the visual examination of the mixture that

Table 2. DSC Data of POSS−DBS Mixtures at Different Weight Ratios Prepared by Solution Mixing (Solution) and Preheating at 200 °C for 5 min (Heated)

			melting transition (T_m, °C)			
components	wt ratio	status	first T_m	second T_m	ΔH (J/g)	T_g (°C)
DBS/tetra-POSS	1:2	solution	broad; 207		116	
	1:2	heated	no melting transition			132
	1:5	solution	broad; 108	broad; 226	59 and 101	
	1:5	heated	no melting transition			214
	1:30	solution	broad; 148	broad; 261	105 and 61	
	1:30	heated	broad; 259		53	
DBS/tri-POSS	1:2	solution	broad; 188		88	
	1:2	heated	no melting transition			151
	1:5	solution	broad; 196		78	
	1:5	heated	no melting transition			106
	1:30	Solution	broad; 142	broad; 210	47 and 47	
	1:30	heated	no melting transition			122
DBS/cyclo-POSS	1:2	solution	broad; 224		138	
	1:2	heated	broad; 242		66	
	1:5	solution	broad; 216		121	
	1:5	heated	broad; 242		122	
	1:30	solution	broad; 232		111	
	1:30	heated	broad; 261		77	

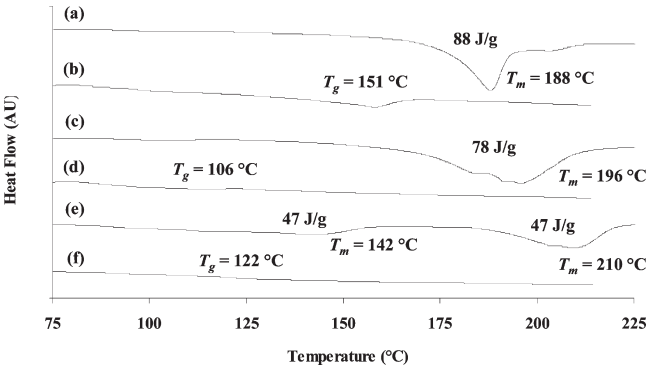

Figure 5. DSC scans (exo up) of DBS/tri-POSS mixtures at various weight ratios: (a) 1:2, (b) 1:2 preheated, (c) 1:5, (d) 1:5 preheated, (e) 1:30, and (f) 1:30 preheated at 200 °C for 5 min. The heat of fusion of the corresponding melting transition is given in J/g.

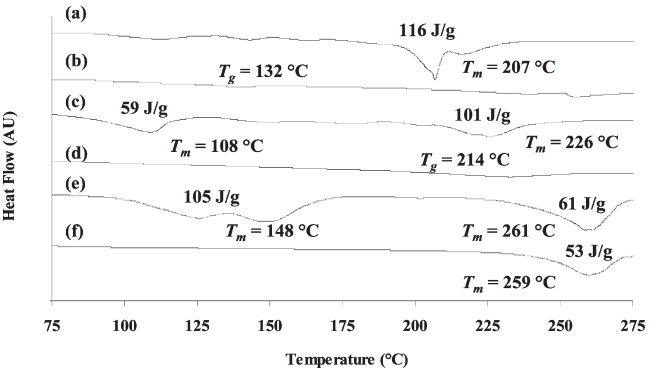

Figure 6. DSC scans (exo up) of DBS/tetra-POSS mixtures at various weight ratios: (a) 1:2, (b) 1:2 preheated, (c) 1:5, (d) 1:5 preheated, (e) 1:30, and (f) 1:30 preheated at 200 °C for 5 min. The heat of fusion of the corresponding melting transition is given in J/g.

excess tetra-POSS beyond 5:1 tetra-POSS/DBS weight ratio remained as solid even at 200 °C. The compounds of DMDBS and POSS were prepared by heating at 210 °C for 5 min. The melting and glass transition temperatures of DMDBS−POSS compounds inferred from DSC traces are presented in S2 of the Supporting Information. It is seen that the trends are similar to DBS systems.

The transformation of mixtures of crystalline tri-POSS or tetra-POSS and DBS into low-viscosity liquid complex upon heating at 200 °C, although somewhat surprising, can be beneficial. First, it generates a liquid with shear viscosity less than 10 Pa·s at 180 °C which will make the liquid amenable to deformation and breakup into small droplets in shear and extensional flows encountered during extrusion, fiber spinning, or film casting of the compounds of iPP, DBS, and tri-POSS or tetra-POSS. Second, the liquid upon solidification generates hard particles for potential reinforcement of the polymer, as already seen in Figure 1. A thorough report on this aspect will be communicated elsewhere. Third, the weight ratio of tri-POSS/DBS or tetra-POSS/DBS can be used to vary the glass transition temperature of the complex to move above or below the crystallization temperature of iPP.

An amorphous material with a T_g of 132 °C (Table 1) was also formed when tri-POSS was heated at 200 °C in the absence of DBS. This phenomenon was reported earlier[23] and was attributed to dehydration/condensation reactions that yielded a mixture of products. These condensations reactions also led to transition of tri-POSS from crystalline to amorphous state as identified previously.[45] However, tetra-POSS retained its crystalline structure after heating at 200 °C, indicating better thermal stability than tri-POSS. Cyclo-POSS also turned amorphous after

heating at 200 °C with a glass transition temperature of 211 °C. However, unlike in the cases of tri-POSS and tetra-POSS, the cyclo-POSS and DBS mixtures heated at 200 °C did not show loss of crystallinity (Table 2). Let us now discuss the origin of two melting peaks seen in the case of solution mixed POSS and DBS.

The DSC traces of tri-POSS and tetra-POSS/DBS mixtures prepared in solution showed broad melting transitions, and the melting peaks appeared at substantially lower temperatures than those of DBS, tri-POSS, and tetra-POSS as reflected in Figures 5 and 6. For example, a 2:1 wt/wt tri-POSS/DBS mixture showed a melting peak at 188 °C although DBS and tri-POSS showed individual melting peaks at 227 °C. The melting peaks moved to higher temperature with the increase of tri-POSS and tetra-POSS content in the mixtures and a second melting peak appeared. For example, two melting peaks, respectively at 210 and 142 °C were observed with 30:1 wt/wt tri-POSS/DBS mixture. A 30:1 wt/wt tetra-POSS/DBS mixture also showed two melting peaks respectively at 148 and 261 °C. The lowering of melting peaks with the addition of DBS to tri-POSS and tetra-POSS can be attributed to good compatibility between DBS and phenyl-substituted silanol-POSS. This was not apparent, however, in cyclo-POSS/DBS mixtures, indicating poor compatibility between these compounds, although shear rheology in Figure 3 indicated some interactions between these molecules.

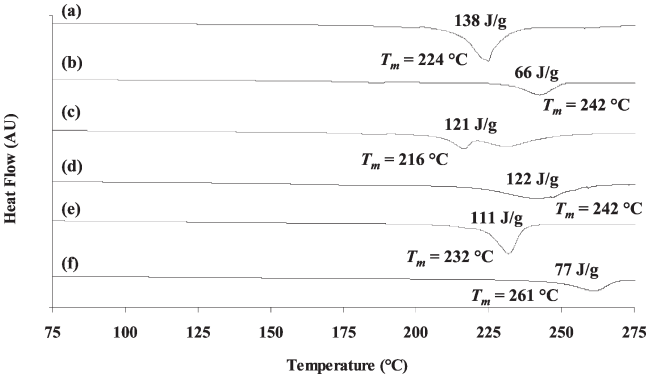

Figure 7. DSC scans (exo up) of DBS/cyclo-POSS mixtures at various weight ratios: (a) 1:2, (b) 1:2 preheated, (c) 1:5, (d) 1:5 preheated, (e) 1:30, and (f) 1:30 preheated at 200 °C for 5 min. The heat of fusion of the corresponding melting transition is given in J/g.

The solid mixtures of silanol−POSS and DBS before and after heating at 200 °C for 5 min were examined by WAXD and their patterns compared with those of silanol-POSS and DBS. Figure 8 presents evidence of the crystalline structure of DBS and various POSS. In addition, these patterns captured the structural changes in preheated silanol−POSS and their mixtures with DBS. The bright arc patterns in Figure 8a,c,e,g are attributed to the crystalline structures of DBS and silanol−POSS. The bright halo in Figure 8f is due to the amorphous nature of preheated tri-POSS which indicates that heating tri-POSS at 200 °C for 5 min destroyed its crystalline structures as was already inferred from the absence of melting peaks in DSC traces. A comparison of the WAXD patterns of DBS and tetra-POSS before and after heat treatment revealed that the crystalline structures were not influenced by the heat treatment. The crystalline structure of cyclo-POSS, however, changed due to heat treatment as evident from Figure 8h.

The bright halo in WAXD patterns in Figure 9 provides evidence that the crystalline, solution mixed tetra- and tri-POSS/DBS mixtures turned amorphous due to heating at 200 °C for 5 min. Only the tetra-POSS/DBS mixture with 30:1 wt/wt ratio showed the existence of small crystals (small bright dots in Figure 9g) before heat treatment. These small crystals supports the broad melting peak observed at ∼150 °C in the DSC traces of solution mixed tetra-POSS/DBS system. After heating, the lower melting transition disappeared (Figure 6) as supported by the bright arc pattern in WAXD in Figure 9h. The cyclo-POSS retained its crystalline nature both for the mixed and preheated samples.

Organization of Silanol−POSS. The organization of silanol−POSS in mixtures with DBS was investigated by SEM. For this purpose, solutions of DBS, POSS, and POSS/DBS mixtures were cast as films on SEM stubs and their morphology compared as presented in Figures 10 and 11. Crystalline DBS formed nanofibrillar networks with diameter ∼20 nm (Figure 10a). Crystalline lamellar structures are also seen for tri-POSS and tetra-POSS respectively in Figure 10b and Figure 10c; the

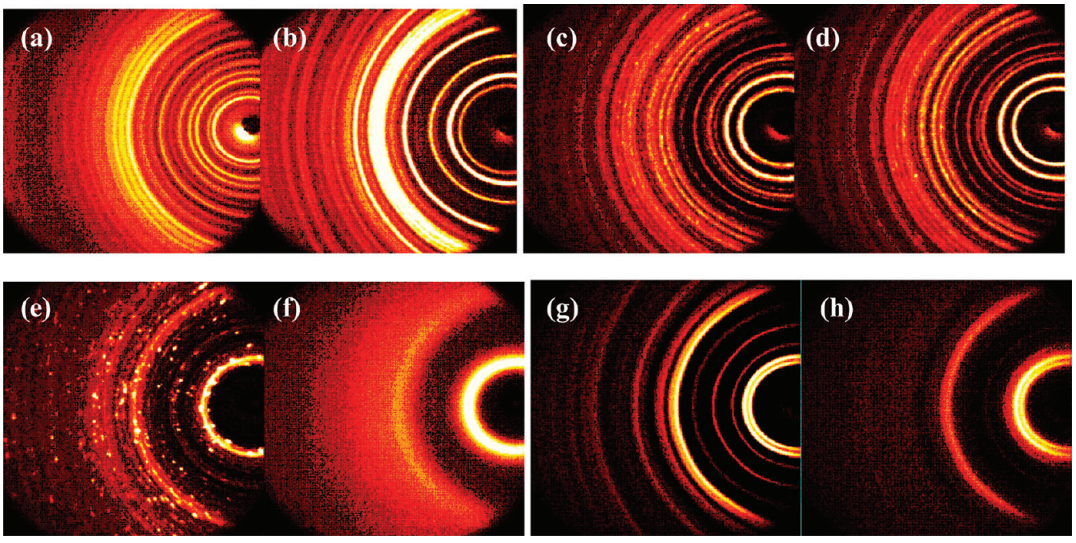

Figure 8. WAXD patterns of (a) DBS, (b) heat-treated DBS, (c) tetra-POSS, (d) tetra-POSS heated, (e) tri-POSS, (f) tri-POSS heated, (g) cyclo-POSS, and (h) cyclo-POSS heated at 200 °C for 5 min.

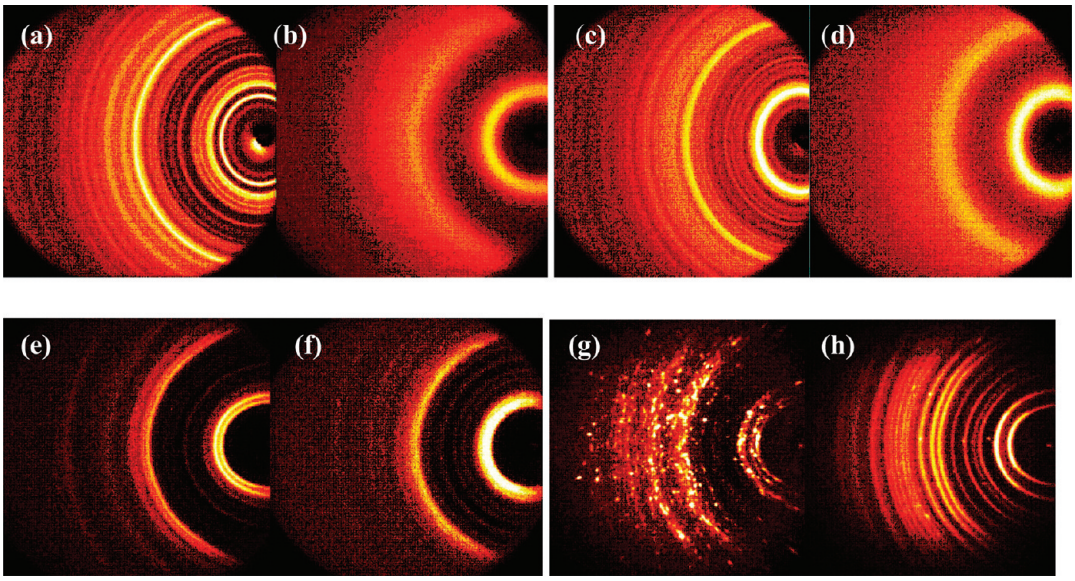

Figure 9. WAXD patterns of (a) DBS/tetra-POSS 1:2 wt/wt, (b) DBS/tetra-POSS 1:2 wt/wt preheated, (c) DBS/tri-POSS 1:2 wt/wt, (d) DBS/tri-POSS 1:2 wt/wt preheated, (e) DBS/cyclo-POSS 1:2 wt/wt, (f) DBS/cyclo-POSS 1:2 wt/wt preheated, (g) DBS/tetra-POSS 1:30 wt/wt, and (h) DBS/tetra-POSS 1:30 wt/wt preheated; at 200 °C for 5 min.

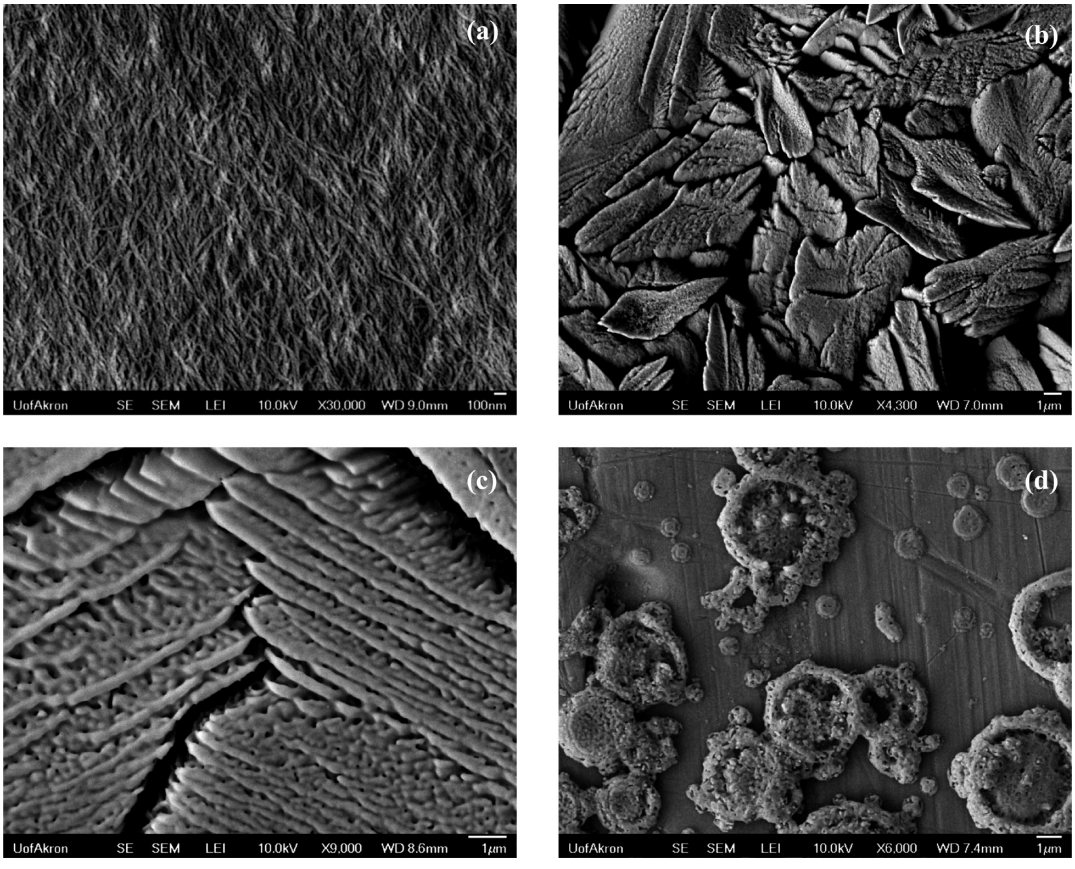

Figure 10. SEM images of DBS and POSS particles as observed from solvent cast system: (a) DBS, (b) tetra-POSS, (c) tri-POSS, and (d) cyclo-POSS.

cyclo-POSS molecules formed circular crystalline domains (Figure 10d). This self-aggregation can be attributed to intermolecular hydrogen bonding between the molecules of silanol−POSS.[24] The phenylsilanol−POSS molecules formed much smaller crystalline aggregates in the presence of DBS (Figure 11a,b) possibly due to mixing and interactions with DBS. The fibrillar domains of DBS are apparent in Figure 11. The smaller crystalline aggregates can explain the depression of

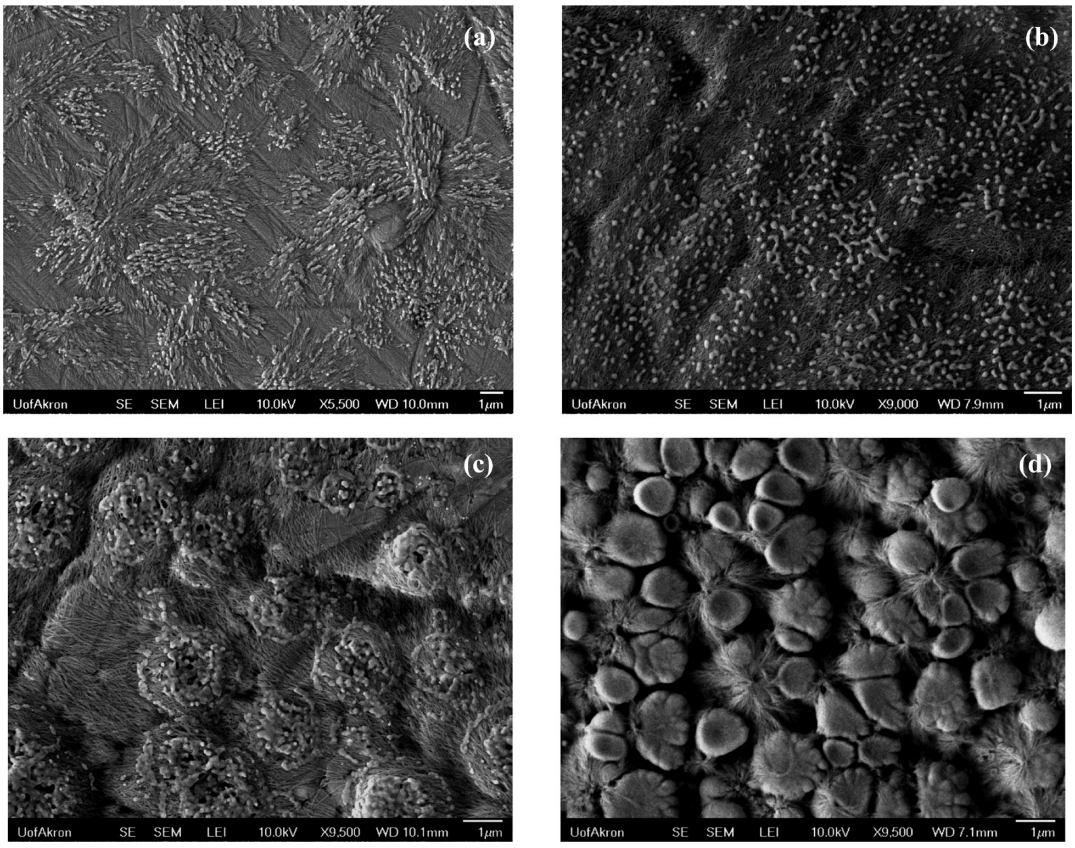

Figure 11. SEM images of DBS and POSS mixtures as observed from solvent cast system: (a) DBS/tetra-POSS, (b) DBS/tri-POSS, (c) DBS/cyclo-POSS, and (d) DBS/cyclo-POSS heated at 200 °C (DBS/POSS 1/2 wt/wt).

melting point observed in Table 2, Figure 5, and Figure 6. Recall that 1:2 wt/wt DBS/tri-POSS mixture showed a melting temperature of 188 °C while the crystalline melting temperatures of DBS and tri-POSS are respectively 227 and 227 °C. The cyclo-POSS domains retained much of its circular shapes when mixed with DBS (Figure 11c), indicating greater POSS−POSS affinity. In this case, the melting temperature depression of cyclo-POSS crystalline domains was not much, e.g., 224 °C for a mixture of 1:2 wt/wt ratio of DBS/cyclo-POSS and 232 °C for a mixture of 1:30 wt/wt DBS/cyclo-POSS (Table 2); the crystalline melting temperature of cyclo-POSS was 242 °C.

The morphological features of DBS, silanol−POSS, and their mixtures were examined after heating these materials at 200 °C for 5 min, and the resultant materials were solution cast on SEM stubs. As already discussed in conjunction with DSC data presented in Table 1, the tri-POSS and cyclo-POSS turned amorphous due to such thermal history and did not show melting transitions while tetra-POSS remained crystalline. Consequently, no distinct morphological features were identified in SEM images of heated materials of tri-POSS or its mixtures with DBS. Although cyclo-POSS became amorphous upon heating, the crystalline POSS domains and DBS fibrils are seen in Figure 11d. This is surprising, since cyclo-POSS did transform into amorphous state due to heating. Therefore, the presence of DBS must have deterred transformation of cyclo-POSS crystals into an amorphous state.

POSS−DBS Molecular Complex from Mass Spectroscopy. The DBS/silanol−POSS mixtures were examined by ESI mass spectrometry to unveil the structures of molecular complexes. The gentle ionization in ESI method is able to retain the noncovalent interactions between the molecules intact during the transfer of the analytes into the gas phase. The resulting mass spectra identified the composition of several complexes formed, such as POSS−POSS, DBS−DBS, and POSS−DBS.

Structure formation in POSS and DBS was investigated first in order to determine the changes before and after heating at 200 °C. Several combinations of POSS−DBS molecules were mixed at different molar ratios and at different temperatures, e.g., at room temperature and at 200 °C for 5 min. The ESI mass spectra of DBS showed the quasi-molecular ions $[M + Na]^+$ as base peaks as well as the respective dimeric species $[2M + Na]^+$ (S3 in Supporting Information). Although no salt was added to the sample solutions, all ions observed were adducts with sodium ions. These ions were possibly derived from the glassware or were present in the as-received samples. Poly(ethylene glycol) (PEG) impurities were also detected in the analyzed DBS and probably originated from the chemical synthesis of DBS.

No change or degradation was evident in the respective mass spectra of DBS after heating at a temperature of 200 °C for 5 min and allowing to cool down to room temperature (Supporting Information S3). This indicates reasonable thermal stability of DBS during compound preparation and rheological measurement.

ESI analysis of the individual POSS materials confirms that such molecules can form noncovalent complexes (see Supporting Information S4). Note that the stoichiometry of the complexes

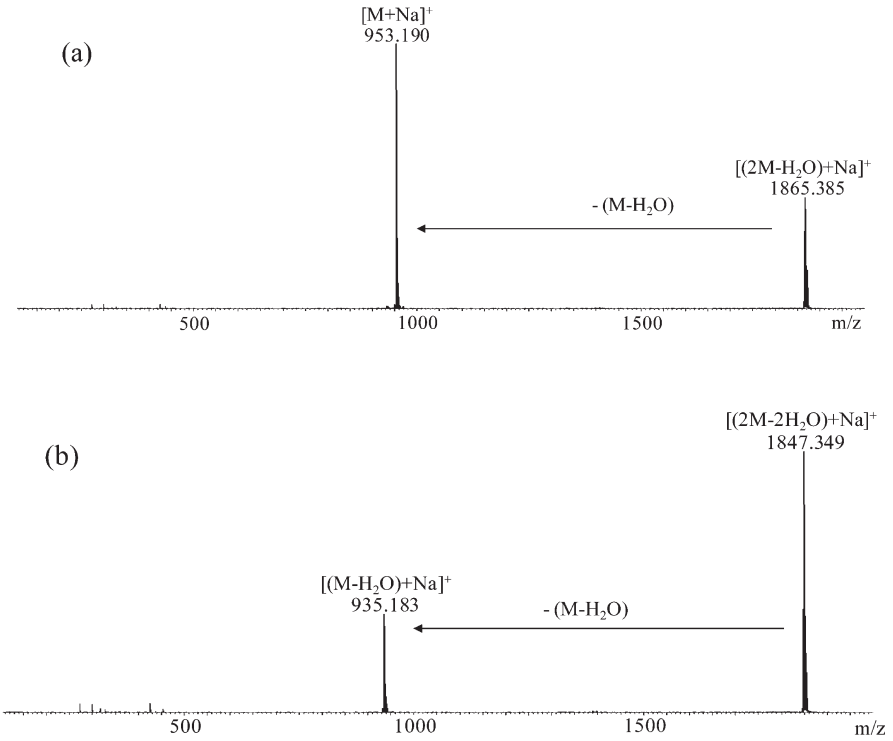

Figure 12. MS/MS spectra of condensation products from tri-POSS heated at 200 °C: (a) $[(2M-H_2O) + Na]^+$ (m/z 1865) fragmented at a collision energy of 17 eV; (b) $[(2M-2H_2O) + Na]^+$ (m/z 1847) fragmented at a collision energy of 20 eV.

detected is up to $[4M + Na]^+$ for tri- POSS, $[3M + Na]^+$ for tetra- POSS, and just $[2M + Na]^+$ for the cyclo-POSS.

The higher degree of complexation observed for tri-POSS and tetra-POSS systems can be rationalized by the hydrogen bonding and additional $\pi-\pi$ stacking interactions derived from the phenyl functionalities, which improve the overall stability of the resulting complexes. The binding interactions in the observed complexes of cyclo-POSS must be the result of hydrogen bonding[23,24] as the molecule does not carry any aromatic side groups. The same POSS molecules underwent some degradation when thermally treated at 200 °C for 5 min. The mass spectra of tri-POSS and cyclo-POSS (see Supporting Information S5) indicate consecutive water losses, pointing out condensation reactions during heating. Note that the number of water molecule losses increased with the complex order, e.g., one water loss from the monomer $[M + Na]^+$, two water losses for the dimer $[2M + Na]^+$, and four water losses from the trimer $[3M + Na]^+$. Additional minor fragments in the spectra, labeled as asterisks, arose from the consecutive elimination of SiPhO and H_2O units. Conversely, no condensation or degradation product was detected for tetra-POSS (see Supporting Information S5).

The tandem mass spectrometry (MS/MS) studies of the ion species arising from water losses confirmed that the condensation reactions indeed occurred in the single POSS molecules via intramolecular condensation rather than between two POSS units, which would have led to covalently bonded POSS units. This was reported earlier[23] and exemplified here in Figure 12, which illustrates the MS/MS spectra of the sodium adducts of $2M-H_2O$ and $2M-2H_2O$ from tri-POSS heated at 200 °C.

Consistent with the noncovalent bonding between the POSS units, relatively low collision energies were necessary to disrupt the complexes, resulting in the loss of a dehydrated POSS unit

Table 3. Self-Assembled Complexes of POSS, DBS, and Their Combinations As Identified from ESI Mass Spectra Analysis

component	status	self-aggregates	intermolecular complexes (POSS/DBS 2/1 wt/wt) exist along with self-aggregates
DBS	RT	mono- and dimer	
	heated	mono- and dimer	
tetra-POSS	RT	mono- to trimer	1:1, 2:1, 3:1
	heated	mono- to trimer	1:1, 2:1, and corresponding dehydrated product
tri-POSS	RT	mono- to trimer	1:1, 2:1, 3:1
	heated	mono- to trimer and dehydrated product	1:1, 2:1, and corresponding dehydrated product
cyclo-POSS	RT	mono- and dimer	1:1
	heated	mono- and dimer dehydrated product	1:1, no dehydrated product from this complex

$(M-H_2O)$ from both the condensation products investigated. In the case of $(2M-2H_2O)$, Figure 12b, the loss of a $(M-H_2O)$ unit to generate a sodiated $(M-H_2O)$ fragment ion indicates that each of the POSS molecules in the complex had undergone one intramolecular condensation reaction. In the same vein, the loss of $(M-H_2O)$ from sodiated $(2M-H_2O)$ to produce

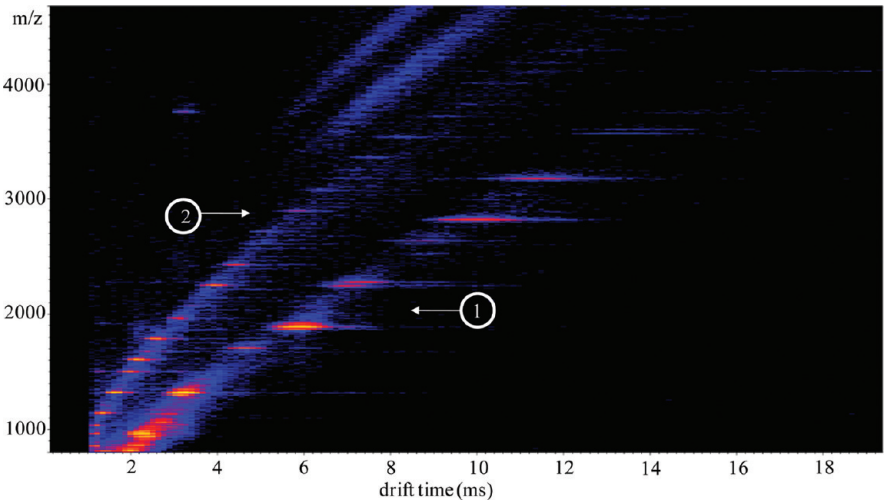

Figure 13. Ion mobility diagram of m/z versus drift time for tri-POSS/DBS (2/1 wt/wt). Band 1 is composed of singly charged complexes (higher drift time), while band 2 represents doubly charged complexes (lower drift time).

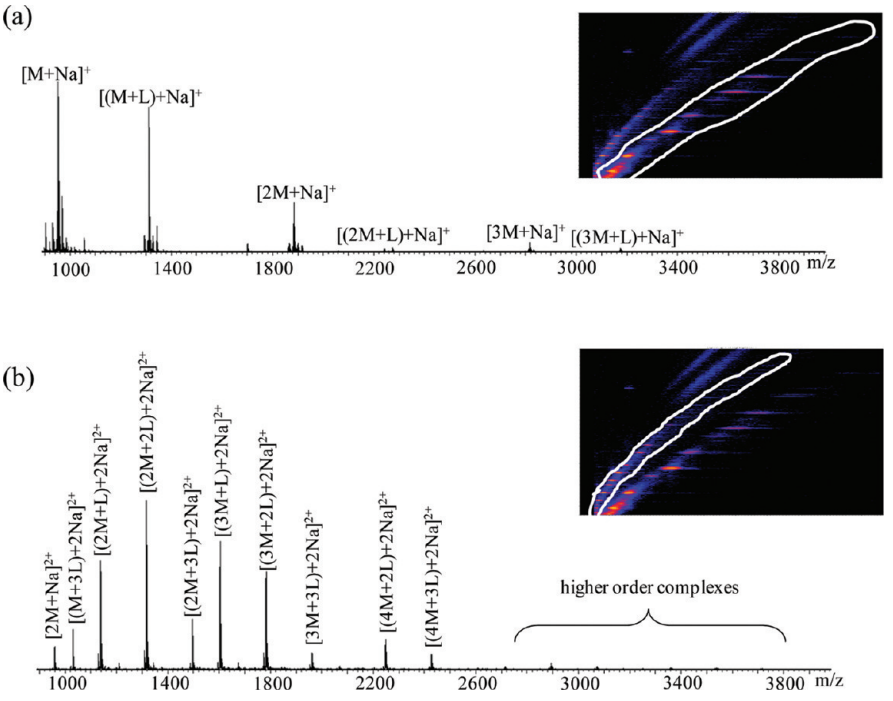

Figure 14. Mass spectra extracted from the different bands of the 2D ion mobility diagram shown in Figure 17. Spectrum (a) corresponds to the band 1 of singly charged complexes; spectrum (b) results from the band 2 of doubly charged complexes.

$[M + Na]^+$ (see Supporting Information S5) confirms that only one of the two POSS molecules had undergone condensation.

Several POSS−DBS and POSS−POSS complexes were detected in the mixtures of POSS and DBS as cited in Table 3. The detection of cyclo-POSS/DBS complexes confirms that hydrogen bonding was responsible for binding interactions between the complex constituents. The POSS−DBS complexes with 1:1 stoichiometry were always the dominant products (see Supporting Information S6). Note that the intensity of the POSS−DBS complexes decreased due to an increase of the molar ratio of POSS and DBS to 30:1. This expected behavior is a consequence of the lower amount of DBS molecules available to interact with the POSS molecules, which can instead self-assemble with themselves.

The investigation of the POSS−DBS systems by ion mobility mass spectrometry (IMMS) unveiled the existence of multiply charged higher order complexes, which could not be identified by traditional MS analysis due to the overlapping of their m/z values with those of other complexes at a different charge state, for example $[(M + L) + Na]^+$ and $[(2M + 2L) + 2Na]^{2+}$ (Figure 13). IMMS has been developed and applied as a method to differentiate isobaric and isomeric constituents of complex mixtures as well as macromolecular architectures such as linear, cyclic, or branched. It can also differentiate species with the same m/z

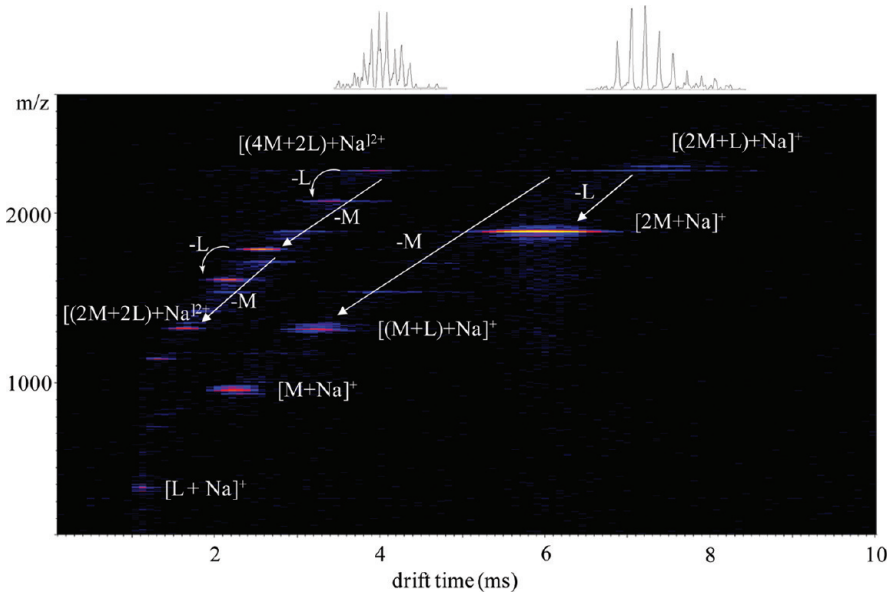

Figure 15. IM MS/MS diagram of the overlapping complexes $[(2M + L) + Na]^+$ and $[(4M + 2L) + 2Na]^{2+}$ from tri-POSS/DBS (2:1).

value but different charge state, which results in a shorter or longer drift time through the ion mobility cell, respectively.[47−50]

The IMMS diagram of tri-POSS/DBS shows two distinct bands, each containing a different charge state of the POSS-DBS complexes: singly charged complexes (band 1) and doubly charged complexes (band 2). Separate integration of each band provides the corresponding 2D mass spectra (Figure 14). Figure 14b illustrates the mass spectrum derived from band 2, which confirms the presence of complexes with a higher stoichiometry compared to the singly charged complexes observed in the spectrum of the band 1 (Figure 14a). The higher charge state of the complexes with a higher number of POSS or sorbitol components arises from the high sodium affinity of the oxygen atoms present on both the sorbitol and POSS molecules.

Additional evidence for the occurrence of higher order complexes was derived by tandem mass spectrometry analysis coupled with ion mobility separation (IM MS/MS). Figure 15 shows the ion mobility diagram obtained by isolation of the complex $[(2M + L) + Na]^+$ (m/z 2241.8) from tri-POSS/DBS, collision-activated dissociation in the following trap cell to disrupt the complex, IM separation of the fragments and remaining precursors, and mass analysis of the ion mixture with the ToF device. Along with the $[(2M + L) + Na]^+$ ion and its fragments, the isobaric $[(4M + 2L) + 2Na]^{2+}$ and its fragments were also detected. The singly charged species $[(2M + L) + Na]^+$ resulted having a longer drift time than the isobaric $[(4M + 2L) + 2Na]^{2+}$ complex because of its lower charge. The losses of ligands from the isobaric parent ions generated isobaric fragment complexes as well, viz. $[(M + L) + Na]^+$ and $[(2M + 2L) + 2Na]^{2+}$. The charge states of precursor ions and fragments are readily determined from the corresponding isotope patterns, revealed by integration of the respective bands.

The mixtures of POSS−DBS underwent extensive condensation reactions when heated at 200 °C. Thus, thermal degradation is observed not only in the POSS−POSS complexes but also in the POSS−DBS complexes (Table 3; see also Supporting Information S7).

The nature of the condensation products in the POSS−DBS complexes was tested by tandem mass spectrometry. The analysis revealed that no bond was created between the POSS and the DBS molecules (Figure 16). Losses of both intact DBS (L) and either POSS or dehydrated POSS molecules confirmed that the condensation occurred in the POSS molecules by intramolecular H_2O elimination, as seen before.

POSS−DBS Reactivity. The chemical reactivity, morphology, and extent of mixing of POSS−DBS were examined using solid-state NMR. Application of solid-state NMR in the analysis of these materials has the advantages that the entire sample is analyzed, not only the components that are vaporized and ionized, and the NMR data are sensitive to the chemical environments on the length scale of ≤1 nm. The solid-state ^{29}Si NMR spectra from tri-POSS, before and after heating, and the tri-POSS-DBS blend are shown in (Figure 17). In ^{29}Si NMR spectra from silica materials it is typical to observe two distinct peaks, with the upfield peak arising from the silica network, $Si(-OSi)_4$ and the downfield peak from surface silica, $Si(-OSi)_3(-OH)$;[51] these species are labeled Q_4 and Q_3, respectively. Since the Si in tri-POSS is directly bonded to a carbon, the ^{29}Si chemical shifts from tri-POSS (−69, −77, and −79 ppm) are downfield relative to those from the silica network[52] and consistent with those reported previously.[53] After heating tri-POSS to 200 °C, the NMR peaks are significantly broader and the relative intensity of the peak at −69 ppm is reduced. This reduction in peak intensity is accounted for by condensation of the Si−OH groups of tri-POSS to form new Si−O−Si sites,[23] reducing the number of Q_3 sites and increasing the number of Q_4 sites in the material. Similar results were also obtained by mass spectrometry, and the dehydration/condensation was shown to be intramolecular (vide supra). The condensation reaction of tri-POSS reduces the structural order of the material, and formation of several complex structures[23] leads to the observed broadening of the peaks in the NMR data. In the ^{29}Si NMR spectrum from the tri-POSS-DBS blend, the peaks are broader than that observed for unheated tri-POSS, indicating a loss of order of the tri-POSS as a result of mixing with the DBS. Dispersion of

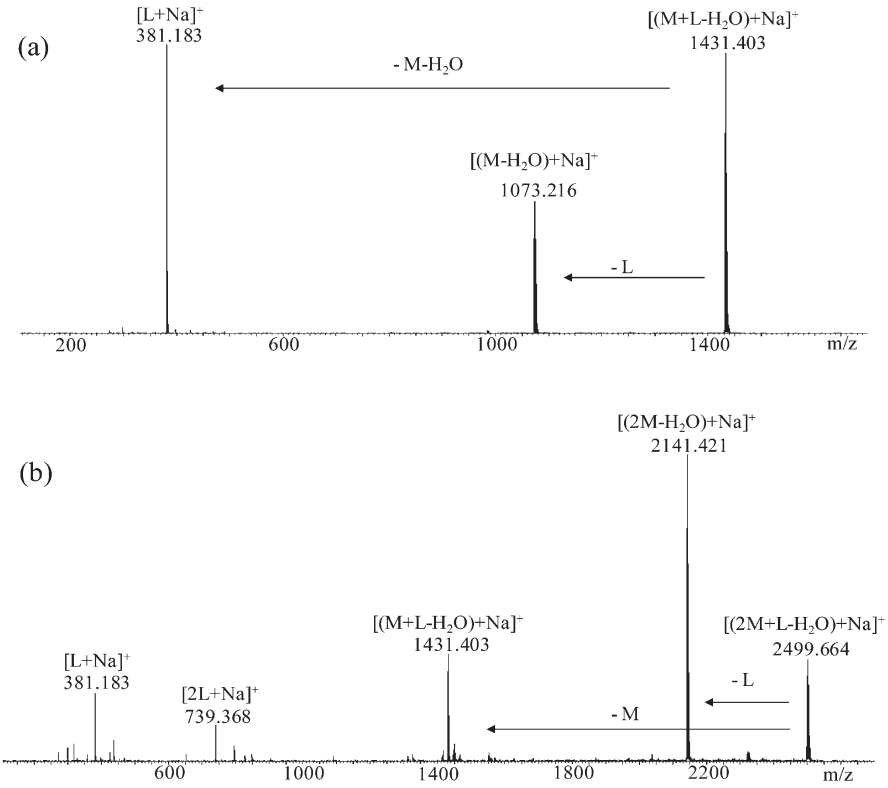

Figure 16. MS/MS spectra of condensation products in the tetra-POSS/DBS mixture heated at 200 °C: (a) $[(M + L{-}H_2O) + Na]^+$ (m/z 1431.4) fragmented at a collision energy of 12 eV; (b) $[(2M + L{-}H_2O) + Na]^+$ (m/z 2499.7) fragmented at a collision energy of 12 eV.

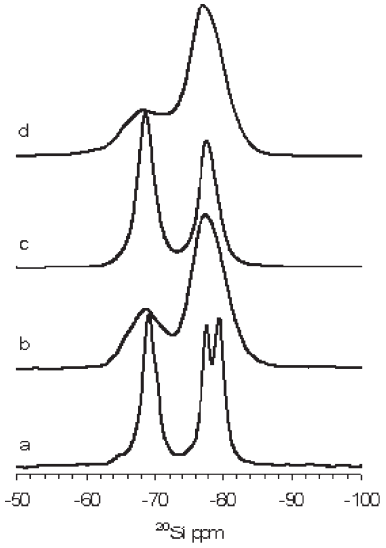

Figure 17. 79.4 MHz $^1H{-}^{29}Si$ CP/MAS SSNMR spectra of (a) tri-POSS, (b) tri-POSS heated at 200 °C, (c) DBS/tri-POSS (1/2 wt/wt), and (d) DBS/tri-POSS (1/2 wt/wt) heated at 200 °C.

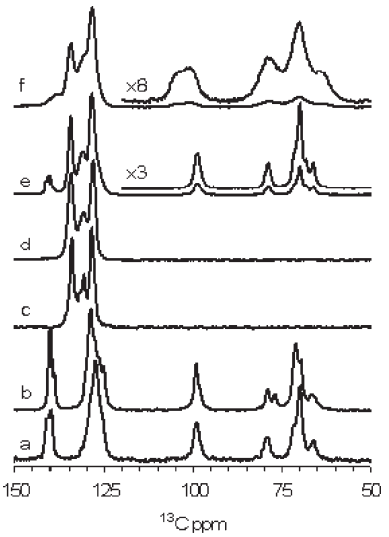

Figure 18. 100.5 MHz $^1H{-}^{13}C$ CP/MAS SSNMR spectra of (a) DBS, (b) DBS heated to 200 °C, (c) tri-POSS, (d) tri-POSS heated at 200 °C, (e) DBS/tri-POSS (1/2 wt/wt), and (f) DBS/tri-POSS (1/2 wt/wt) heated at 200 °C.

tri-POSS within a polymer matrix yielded similar changes in the ^{29}Si NMR line widths.[53]

After heating the mixture at 200 °C, the ^{29}Si NMR spectrum is similar to that observed for heated tri-POSS alone, showing that the Si−OH groups of tri-POSS also underwent condensation in the blend. The NMR data, however, do not show any evidence of reactivity between DBS and tri-POSS, before or after heating, and these results are consistent with those discussed previously.

The tri-POSS/DBS system was further characterized by ^{13}C solid-state NMR (Figure 18). In the ^{13}C NMR spectra from tri-POSS the peaks from the carbons of the phenyl ring occur from 128 to 134 ppm. The peaks are slightly broader after heating the material to 200 °C, and this broadening arises from increased structural heterogeneity resulting from the reactivity of the Si−OH groups, as discussed above. The ^{13}C spectrum from DBS has

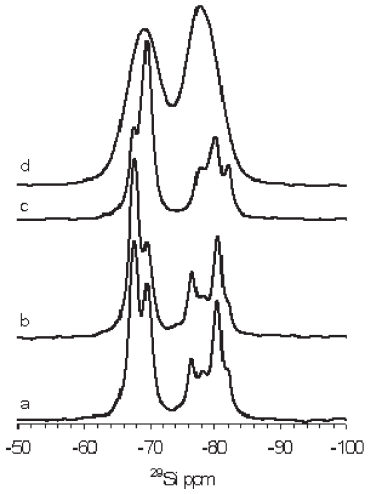

Figure 19. 79.4 MHz $^{1}H-^{29}Si$ CP/MAS SSNMR spectra of (a) tetra-POSS, (b) tetra-POSS heated at 200 °C, (c) DBS/tetra-POSS (1/2 wt/wt), and (d) DBS/tetra-POSS (1/2 wt/wt) heated at 200 °C.

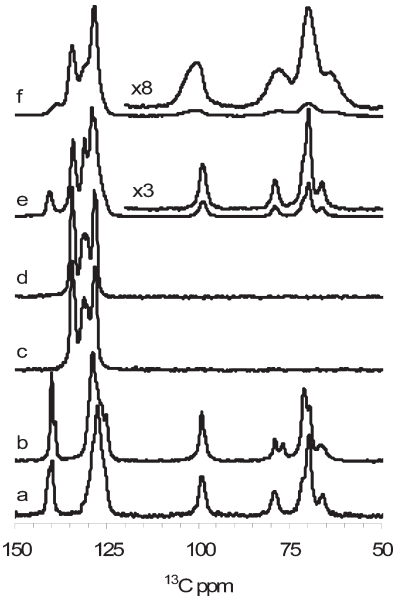

Figure 20. 100.5 MHz $^{1}H-^{13}C$ CP/MAS SSNMR spectra of (a) DBS, (b) DBS heated at 200 °C, (c) tetra-POSS, (d) tetra-POSS heated at 200 °C, (e) DBS/tetra-POSS (1/2 wt/wt), and (f) DBS/tetra-POSS (1/2 wt/wt) heated at 200 °C.

peaks from the phenyl groups at 140 and 127 ppm, carbons next to two oxygen near 100 ppm, and aliphatic ring carbons from 80 to 65 ppm. After heating, there are only small changes in peak shape and relative intensities in the NMR spectrum from pure DBS and these changes likely arise from changes in packing of the molecules upon heating. Substantial reactivity of DBS at 200 °C appears unlikely as no new peaks, arising from reaction products, are observed in the ^{13}C NMR spectrum. The ^{13}C spectrum from the tri-POSS/DBS blend is little different from the sum of the spectra from tri-POSS and DBS themselves, indicating no reactivity between the two species with mixing. Upon heating the mixture, there are no new peaks in the spectra, indicating a lack of reactivity between DBS and tri-POSS. A dehydration reaction between the Si−OH groups of tri-POSS and the alcohol groups of DBS, generating Si−O−C, will generate a new peak near 57 ppm in the ^{13}C spectrum;[54] no peak is observed at this chemical shift. The broadening of the peaks from both DBS, and to a lesser extent tri-POSS, results from a disruption in the packing of the two species, as also observed by WXRD. These results show a mixing of the tri-POSS and DBS and the level of mixing will be discussed below.

The ^{29}Si SSNMR data from the tetra-POSS/DBS system (Figure 19) are similar to the tri-POSS/DBS system, with the peaks from −66 to −71 ppm and −75 to −83 ppm arising from Q_3 and Q_4 Si, respectively. The complex patterns in the spectra from tetra-POSS, similar to those reported previously,[53,55] show that in the solid state the different Si sites are in slightly different chemical environments. The narrow line widths observed are consistent with the crystalline morphology of this material. In contrast to tri-POSS, there is little effect on the spectrum of tetra-POSS upon heating, showing that there was no significant amount of the condensation reaction between Si−OH groups to form additional Si−O−Si linkages. The mixing of tetra-POSS and DBS resulted in only small changes in chemical shifts and line widths, which is in contrast to the tri-POSS system. Since the ^{29}Si NMR spectrum from tetra-POSS in the mixture is very similar to the spectrum from the neat material, the mixture was heterogeneous and contained domains of tetra-POSS. Upon heating the mixture, the peaks in the ^{29}Si NMR were broadened significantly, indicating a loss of the crystallinity of the tretra-POSS domains, consistent with the observation from the WXRD studies. The similar integrated intensities of the two peaks, or two groups of peaks, in all the ^{29}Si NMR data show that the condensation of tetra-POSS does not occur upon mixing with DBS or with heating the blend to 200 °C.

The ^{13}C NMR spectra from tetra-POSS and tetra-POSS in a mixture with DBS (Figure 20) show very similar chemical shifts and line widths to those observed for the tri-POSS/DBS material (Figure 18). Heating tetra-POSS resulted in only small changes in line widths, similar to the ^{29}Si NMR data, confirming the lack of reactivity and changes in the solid-state packing at elevated temperatures. In the case of the blend, a small increase in the ^{13}C NMR line widths was observed for the peaks from both the aromatic carbons of tetra-POSS and the carbons of DBS, mirroring the changes observed in the ^{29}Si NMR data from the mixture. After heating the mixture to 200 °C, the line widths in the ^{13}C NMR spectrum from the mixture were significantly broader, as observed in the corresponding ^{29}Si NMR data. This large increase in line width corresponds to a conversion of the material from a crystalline or near-crystalline morphology to an amorphous state as was inferred from DSC and WAXD. This morphological change was not accompanied by a chemical reaction as a peak near 57 ppm, from the dehydration reaction between tetra-POSS and DBS, is not observed.

The extensive broadening of the peaks in the ^{13}C NMR data after heating mixtures of DBS with tri-POSS and tetra-POSS indicates a disruption of the packing morphologies. Similarly, the DSC studies show that while a melting transition is observed for DBS and the two POSS derivatives, no transition is observed for mixtures that had been heated. While the DSC results show that the DBS and POSS are mixed, this technique has a resolution of 10−50 nm, depending on the material being studied.[56,57] Mixtures containing domains with sizes on the order of tens of nanometers would be expected to produce NMR data that are not dissimilar from the neat material, as is observed for the ^{29}Si data from tetra-POSS in a mixture with DBS. The NMR studies

show that for the materials studied here the increase in line widths in the ^{13}C and ^{29}Si NMR data after heating is consistent with miscibility of POSS derivatives and DBS and mixing at the molecular level. The dominant intermolecular interaction is expected to be hydrogen bonding between the −OH groups, and since hydrogen bonding will lead to only small changes in chemical shifts in the ^{13}C NMR data, these shifts would not be detected in the presence of the large line widths observed.

CONCLUSIONS

This study showed that the molecules of silanol−POSS and a sorbitol derivative were capable of forming several complex molecular adducts. Such complex formation occurred due to noncovalent interactions, such as hydrogen bonding. Mass and NMR spectroscopy data revealed the absence of covalent bond formation between silanol−POSS and sorbitol, although tri-POSS and cyclo-POSS underwent intramolecular condensation of silanol groups. The complex formation was more abundant with higher number of silanol groups per molecule of POSS. The molecular adducts were amorphous at room temperature and turned into liquids above the crystalline melting temperature of iPP with almost 3 orders of magnitude lower viscosity than iPP melt. The molecular complex formation prevented fibrillation of the sorbitol derivative used in the study. The results indicate that other organic molecules carrying multiple alcoholic −OH groups may also form such molecular complex with silanol−POSS.

ASSOCIATED CONTENT

Supporting Information. FTIR spectra of POSS, DBS, and their mixture at room temperature (S1); table of DSC analysis of POSS with DMDBS at different weight ratios (S2); ESI mass spectra of DBS as-received and heat-treated samples (S3); ESI mass spectra of various POSS (S4); ESI mass spectra of preheated POSS samples (S5); ESI mass spectra of POSS/DBS mixtures (S6); ESI mass spectra of POSS/DBS preheated mixtures (S7). This material is available free of charge via the Internet at http://pubs.acs.org.

AUTHOR INFORMATION

Corresponding Author

*E-mail janas@uakron.edu, Ph (330) 972-8293, Fax (330) 258-2339.

ACKNOWLEDGMENT

The authors thank the National Science Foundation for providing financial support through Grant CMMI-0727231 and Hybrid Plastics for partnership and FHR Plastics and Milliken Chemicals for assistance with the materials. S.C.J. acknowledges David A. Schiraldi of Case Western Reserve University for introducing him to POSS and for numerous discussions on the subject. Special thanks to Dr. Bojie Wang from The Department of Polymer Science, The University of Akron, for his guidance regarding morphology characterization.

REFERENCES

(1) Fina, A.; Tabuani, D.; Frache, A.; Camino, G. *Polymer* **2005**, *46*, 7855–7866.

(2) Fu, B. X.; Yang, L.; Somani, R. H.; Zong, S. X.; Hsiao, B. S.; Phillips, S.; Blanski, R.; Ruth, P. *J. Polym. Sci., Part B: Polym. Phys.* **2001**, *39*, 2727–2739.

(3) Fu, B. X.; Gelfer, M. Y.; Hsiao, B. S.; Phillips, S.; Viers, B.; Blanski, R.; Ruth, P. *Polymer* **2003**, *44*, 1499–1506.

(4) Huang, J.-C.; He, C.-B.; Xiao, Y.; Mya, K. Y.; Dai, J.; Siow, Y. P. *Polymer* **2003**, *44*, 4491–4499.

(5) Jeon, H. G.; Mather, P. T.; Haddad, T. S. *Polym. Int.* **2000**, *49*, 453–457.

(6) Lee, Y.-J.; Kuo, S.-W.; Huang, W.-J.; Lee, H.-Y.; Chang, F.-C. *J. Polym. Sci., Part B: Polym. Phys.* **2004**, *42*, 1127–1136.

(7) Leu, C.-M.; Chang, Y.-T.; Wei, K.-H. *Macromolecules* **2003**, *36*, 9122–9127.

(8) Mantz, R. A.; Jones, P. F.; Chaffee, K. P.; Lichtenhan, J. D.; Gilman, J. W.; Ismail, I. M. K.; Burmeister, M. J. *Chem. Mater.* **1996**, *8*, 1250–1259.

(9) Misra, R.; Fu, B. X.; Morgan, S. E. *J. Polym. Sci., Part B: Polym. Phys.* **2007**, *45*, 2441–2455.

(10) Phillips, S. H.; Haddad, T. S.; Tomczak, S. J. *Curr. Opin. Solid State Mater. Sci.* **2004**, *8*, 21–29.

(11) Pracella, M.; Chionna, D.; Fina, A.; Tabuani, D.; Frache, A.; Camino, G. *Macromol. Symp.* **2006**, *234*, 59–67.

(12) Xu, H.; Kuo, S.-W.; Lee, J.-S.; Chang, F.-C. *Polymer* **2002**, *43*, 5117–5124.

(13) Yoon, K. H.; Polk, M. B.; Park, J. H.; Min, B. G.; Schiraldi, D. A. *Polym. Int.* **2005**, *54*, 47–53.

(14) Zeng, J.; Kumar, S.; Iyer, S.; Schiraldi, D. A.; Gonzalez, R. I. *High Perform. Polym.* **2005**, *17*, 403–424.

(15) Wu, J.; Haddad, T. S.; Kim, G.-M.; Mather, P. T. *Macromolecules* **2007**, *40*, 544–554.

(16) Zhao, Y.; Schiraldi, D. A. *Polymer* **2005**, *46*, 11640–11647.

(17) Zheng, L.; Farris, R. J.; Coughlin, E. B. *Macromolecules* **2001**, *34*, 8034–8039.

(18) Zheng, L.; Hong, S.; Cardoen, G.; Burgaz, E.; Gido, S. P.; Coughlin, E. B. *Macromolecules* **2004**, *37*, 8606–8611.

(19) Fasce, D. P.; Williams, R. J. J.; Mechin, F.; Pascault, J. P.; Llauro, M. F.; Petiaud, R. *Macromolecules* **1999**, *32*, 4757–4763.

(20) Sellinger, A.; Laine, R. M. *Macromolecules* **1996**, *29*, 2327–30.

(21) Wu, J.; Mather, P. T. *Polym. Rev. (Philadelphia, PA, U. S.)* **2009**, *49*, 25–63.

(22) Kuo, S.-W.; Lin, H.-C.; Huang, W.-J.; Huang, C.-F.; Chang, F.-C. *J. Polym. Sci., Part B: Polym. Phys.* **2005**, *44*, 673–686.

(23) Feher, F. J.; Newman, D. A.; Walzer, J. F. *J. Am. Chem. Soc.* **1989**, *111*, 1741–8.

(24) Liu, H.; Kondo, S.-i.; Tanaka, R.; Oku, H.; Unno, M. *J. Organomet. Chem.* **2008**, *693*, 1301–1308.

(25) Feher, F. J.; Terroba, R.; Ziller, J. W. *Chem. Commun.* **1999**, 2309–2310.

(26) Lichtenhan, J. D.; Schwab, J. J.; Reinerth, W.; Carr, M. J.; An, Y.-z.; Feher, F. J.; Terroba, R. (Hybrid Plastics, USA). Application: WO WO, 2001; p 45.

(27) Shockey, E. G.; Bolf, A. G.; Jones, P. F.; Schwab, J. J.; Chaffee, K. P.; Haddad, T. S.; Lichtenhan, J. D. *Appl. Organomet. Chem.* **1999**, *13*, 311–327.

(28) Li, Z.; Kawakami, Y. *Chem. Lett.* **2008**, *37*, 804–805.

(29) Cooke, G.; Rotello, V. M. *Chem. Soc. Rev.* **2002**, *31*, 275–286.

(30) Chandrasekhar, V.; Boomishankar, R.; Nagendran, S. *Chem. Rev.* **2004**, *104*, 5847–910.

(31) Thierry, A.; Fillon, B.; Straupe, C.; Lotz, B.; Wittmann, J. C. *Prog. Colloid Polym. Sci.* **1992**, *87*, 28–31.

(32) Libster, D.; Aserin, A.; Garti, N. *Polym. Adv. Technol.* **2007**, *18*, 685–695.

(33) Thierry, A.; Straupe, C.; Lotz, B.; Wittmann, J. C. *Polym. Commun.* **1990**, *31*, 299–301.

(34) Smith, T. L.; Masilamani, D.; Bui, L. K.; Khanna, Y. P.; Bray, R. G.; Hammond, W. B.; Curran, S.; Belles, J. J., Jr.; Binder-Castelli, S. *Macromolecules* **1994**, *27*, 3147–55.

(35) Kristiansen, M.; Werner, M.; Tervoort, T.; Smith, P.; Blomenhofer, M.; Schmidt, H.-W. *Macromolecules* **2003**, *36*, 5150–5156.

(36) Watase, M.; Nakatani, Y.; Itagaki, H. *J. Phys. Chem. B* **1999**, *103*, 2366–2373.

(37) Wilder, E. A.; Spontak, R. J.; Hall, C. K. *Mol. Phys.* **2003**, *101*, 3017–3027.
(38) Shepard, T. A.; Delsorbo, C. R.; Louth, R. M.; Walborn, J. L.; Norman, D. A.; Harvey, N. G.; Spontak, R. J. *J. Polym. Sci., Part B: Polym. Phys.* **1997**, *35*, 2617–2628.
(39) Vaughan, A. S.; Hosier, I. L. *J. Mater. Sci.* **2008**, *43*, 2922–2928.
(40) Brown, J. F., Jr.; Vogt, L. H., Jr. *J. Am. Chem. Soc.* **1965**, *87*, 4313–17.
(41) Feher, F. J.; Phillips, S. H.; Ziller, J. W. *Chem. Commun.* **1997**, 829–830.
(42) Lee, B.-J.; Jana, S. C. *Annu. Tech. Conf.—Soc. Plast. Eng.* **2008**, *66*, 177–181.
(43) Lee, B.-J.; Roy, S.; Jana, S. C. *Annu. Tech. Conf.—Soc. Plast. Eng.* **2009**, *67*, 126–130.
(44) Perilla, J. E.; Lee, B.-J.; Jana, S. C. *J. Rheol.* **2010**, *54*, 761–779.
(45) Lee, B.-J. Dissertation, University of Akron, 2009.
(46) Pringle, S. D.; Giles, K.; Wildgoose, J. L.; Williams, J. P.; Slade, S. E.; Thalassinos, K.; Bateman, R. H.; Bowers, M. T.; Scrivens, J. H. *Int. J. Mass Spectrom.* **2007**, *261*, 1–12.
(47) Kanu, A. B.; Dwivedi, P.; Tam, M.; Matz, L.; Hill, H. H., Jr. *J. Mass Spectrom.* **2008**, *43*, 1–22.
(48) Bowers, M. T.; Kemper, P. R.; von Helden, G.; van Koppen, P. A. M. *Science* **1993**, *260*, 1446–51.
(49) Clemmer, D. E.; Jarrold, M. F. *J. Mass Spectrom.* **1997**, *32*, 577–592.
(50) Trimpin, S.; Plasencia, M.; Isailovic, D.; Clemmer, D. E. *Anal. Chem.* **2007**, *79*, 7965–7974.
(51) Lippmaa, E.; Maegi, M.; Samoson, A.; Engelhardt, G.; Grimmer, A. R. *J. Am. Chem. Soc.* **1980**, *102*, 4889–93.
(52) *Solid-State NMR Spectroscopy of Inorganic Materials*; Fitzgerald, J. J., Ed.; American Chemical Society: Washington, DC, 1999; Vol. 717.
(53) Misra, R.; Alidedeoglu, A. H.; Jarrett, W. L.; Morgan, S. E. *Polymer* **2009**, *50*, 2906–2918.
(54) Rakita, P. E.; Worsham, L. S.; Srebro, J. P. *Org. Magn. Reson.* **1976**, *8*, 310–16.
(55) Hay, M. T.; Seurer, B.; Holmes, D.; Lee, A. *Macromolecules* **2010**, *43*, 2108–2110.
(56) Kammer, H. W. K., J.; Kummerloewe, C. *Adv. Polym. Sci.* **1993**, *106*, 31–85.
(57) Kaplan, D. S. *J. Appl. Polym. Sci.* **1976**, *20*, 2615–29.